Theoretical investigation of the quasiparticle dispersion of bilayer high-T_c superconductors

Jian-Xin Li,[1,2,3] T. Zhou,[1] and Z. D. Wang[1,2]
[1]*National Laboratory of Solid State Microstructures and Department of Physics, Nanjing University, Nanjing 210093, China*
[2]*Department of Physics & Center of Theoretical and Computational Physics, The University of Hong Kong, Pokfulam Road, Hong Kong, China*
[3]*The Interdisciplinary Center of Theoretical Studies, CAS, Beijing, China*
(Received 21 July 2005; published 27 September 2005)

The renormalization of quasiparticle (QP) dispersion in bilayer high-T_c cuprates is investigated theoretically by examining, respectively, the interactions of the QP with spin fluctuations and phonons. It is illustrated that both interactions are able to give rise to a kink in the dispersion around the antinodes [near $(\pi,0)$]. However, remarkable differences between the two cases are found for the peak/dip/hump structure in the line shape, the QP weight, and the interlayer coupling effect on the kink, which are suggested to serve as a discriminance to single out the dominant interaction in the superconducting state. A comparison to recent photoemission experiments shows clearly that the coupling to the spin resonance is dominant for the QP around antinodes in bilayer systems.

DOI: 10.1103/PhysRevB.72.094515 PACS number(s): 74.25.Jb, 74.72.Hs, 79.60.Bm

The elucidation of many-body interactions in high-T_c superconductors (HTSC's) is considered as an essential step toward an insightful understanding of their superconductivity. Angle-resolved photoemission spectroscopy (ARPES) has provided a powerful way to probe the coupling of charge quasiparticles (QP's) to other QP's or collective modes. Recent ARPES experiments have unveiled several intriguing features in the dispersion, the QP weight, and the line shape: (i) A kink in the dispersion was observed in both the nodal and antinodal regions.[1–4] (ii) The QP weight around the antinodal region decreases rapidly with the reduction of dopings,[5] while it changes a little around the nodal direction.[6] (iii) After disentangling the bilayer splitting effect, an intrinsic peak/dip/hump (PDH) structure is seen around the antinodal region both in the bonding (BB) and antibonding (AB) bands.[2,3] (iv) The kink around the antinodal region seemingly shows a different momentum, temperature, and doping dependence from that around the nodal direction.[2] (v) The antinodal kink is likely absent (or very weak) in the single-layered Bi2201.[4] These features, especially (i), imply that the QP is coupled to a collective mode. So far, two collective modes of 41 meV spin resonance[7,8] and ~36 meV phonons[9,10] have been suggested, but which one is a key factor responsible for the kink is still much debatable.[1–4,9–11] So it raises an important question as to whether the electronic interaction alone is responsible for the intriguing QP dispersion or to what extent the antinodal (nodal) QP's properties are determined by the strong electronic interaction.

In this paper, we not only answer the above important question but also present a coherent understanding of the above features by studying in detail the respective effects of the fermion–spin-fluctuation (SF) interaction and fermion-phonon interaction on the QP dispersion based on the slave-boson theory of the bilayer t-t'-J model. We find that though both couplings are able to give rise to the kink structure near the antinodal region in the QP dispersion, they differ remarkably in the following aspects. (a) The line shape arising from the spin resonance coupling exhibits a clear PDH structure, while the phonon coupling would lead to a reversed PDH structure; namely, the peak is in a larger binding energy than the hump. (b) The former coupling causes a rapid drop of the QP weight near the antinodal region with underdoping, but the latter has only a very weak effect. Moreover, the corresponding coupling constant for the fermion-SF interaction is reasonable consistent with ARPES data, in contrast to the much smaller value for the fermion-phonon interaction. (c) The bilayer coupling plays a positive role in the occurrence of the kink in the case of the fermion-SF interaction, but has a negative effect on the formation of the kink for the fermion-phonon interaction. These results suggest that the SF coupling is a dominant interaction involved in the antinode-to-antinode scattering.

We will consider separately the interactions of fermions with the SF and phonons. Let us start with the bilayer t-t'-J model with the AF interaction included,

$$H = -\sum_{\langle ij\rangle\alpha\alpha'\sigma} t_{\alpha,\alpha'} c_{i\sigma}^{(\alpha)\dagger} c_{j\sigma}^{(\alpha')} - \sum_{\langle ij\rangle'\alpha\sigma} t' c_{i\sigma}^{(\alpha)\dagger} c_{j\sigma}^{(\alpha)} - \text{H.c.} + \sum_{\langle ij\rangle\alpha\alpha'} J_{\alpha,\alpha'} \mathbf{S}_i^{(\alpha)} \cdot \mathbf{S}_j^{(\alpha')}, \quad (1)$$

where $\alpha=1,2$ denotes the layer index, $t_{\alpha,\alpha'}=t$, $J_{\alpha,\alpha'}=J$ if $\alpha=\alpha'$, otherwise, $t_{\alpha,\alpha'}=t_p/2$, $J_{\alpha,\alpha'}=J_\perp$, and $i=j$. Other symbols are standard. In the slave-boson representation, the electron operators $c_{j\sigma}$ are written as $c_{j\sigma}=b_j^\dagger f_{j\sigma}$, where fermions $f_{i\sigma}$ carry spin and bosons b_i represent the charge. Using the mean-field parameters $\chi_{ij}=\Sigma_\sigma\langle f_{i\sigma}^\dagger f_{j\sigma}\rangle=\chi_0$, $\Delta_{ij}=\langle f_{i\uparrow}f_{j\downarrow}-f_{i\downarrow}f_{j\uparrow}\rangle=\pm\Delta_0$, and setting $b\to\sqrt{\delta}$ with δ the doping density (boson condense), we can decouple the Hamiltonian (1). Its Fourier transformation is given by

$$H_m = \sum_{\mathbf{k}\sigma\alpha}\varepsilon_{\mathbf{k}} f_{\mathbf{k}\sigma}^{(\alpha)\dagger} f_{\mathbf{k}\sigma}^{(\alpha)} - \sum_{\mathbf{k}\alpha}\Delta_{\mathbf{k}}(f_{\mathbf{k}\uparrow}^{(\alpha)\dagger} f_{-\mathbf{k}\downarrow}^{(\alpha)\dagger} + \text{H.c.}) + \sum_{\mathbf{k}\sigma}[\delta t_{\perp\mathbf{k}} e^{ik_z c} f_{\mathbf{k}\sigma}^{(1)\dagger} f_{\mathbf{k}\sigma}^{(2)} + \text{H.c.}] + \varepsilon_0,$$

with $\varepsilon_{\mathbf{k}} = -2(\delta t + J'\chi_0)(\cos k_x + \cos k_y) - 4\delta t' \cos k_x \cos k_y$

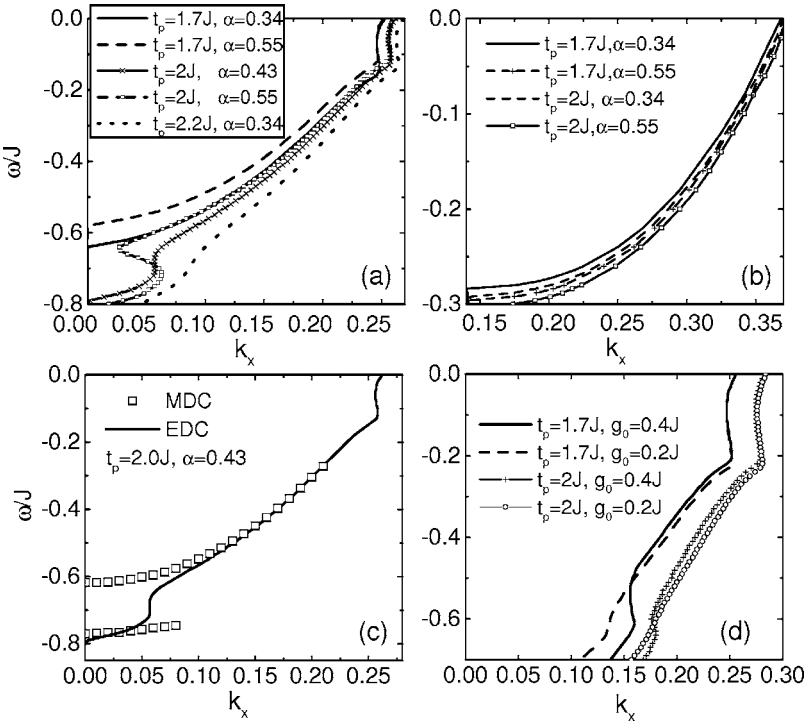

FIG. 1. The MDC dispersion of fermions due to the interaction with spin fluctuations (a),(b),(c) and phonons (d). (a), (c), and (d) are the results at (k_x,π) (antinodal region) and (b) at (k_x,k_x) (nodal direction). The scattered points in (c) are derived from the EDC (Ref. 16).

$-\mu_f$, $\Delta_k=2J'\Delta_0(\cos k_x-\cos k_y)$, $\varepsilon_0=4NJ'(\chi_0^2+\Delta_0^2)$, $t_{\perp\mathbf{k}}=t_p(\cos k_x-\cos k_y)^2/4$ (Ref. 12), and $J'=3J/8$. Diagonalizing the Hamiltonian, we get the AB and BB bands with the dispersion $\epsilon^{(A,B)}=\varepsilon_{\mathbf{k}}\pm\delta t_{\perp\mathbf{k}}$. Then, the bare normal (abnormal) Green's functions of fermions $\mathcal{G}_s^{(A,B)}$ ($\mathcal{G}_w^{(A,B)}$) and the bare spin susceptibility $\chi^{\alpha,\alpha'}(\alpha,\alpha'=A,B)$ are obtained. The physical spin susceptibility is given by $\chi=\chi_0^+\cos^2(q_zc/2)+\chi_0^-\sin^2(q_zc/2)$, with $\chi_0^+=\chi^{AA}+\chi^{BB}$ and $\chi_0^-=\chi^{AB}+\chi^{BA}$.

The slave-boson mean-field theory underestimates the AF correlation,[13,14] so we need to go beyond it and include the effect of SF through the random-phase approximation (RPA), in which the renormalized spin susceptibility is

$$\chi^{\pm}(\mathbf{q},\omega)=\chi_0^{\pm}(\mathbf{q},\omega)/[1+(\alpha J_{\mathbf{q}}\pm J_\perp)\chi_0^{\pm}(\mathbf{q},\omega)/2]. \quad (2)$$

However, in the ordinary RPA ($\alpha=1$), the AF correlation is overestimated as indicated by a larger critical doping density $\delta\approx0.22$ for the AF instability than the experimental data $\delta_c=0.02\sim0.05$.[15] Thus, we use the renormalized RPA in which the parameter α is determined by setting the AF instability at the experimental value δ_c. The fermionic self-energy coming from the SF coupling is given by

$$\Sigma_{s,w}^{(A,B)}(\mathbf{k})=\pm\frac{1}{4N\beta}\sum_{\mathbf{q}}[(J_{\mathbf{q}}+J_\perp)^2\chi^+(\mathbf{q})\mathcal{G}_{s,w}^{(A,B)}(\mathbf{k}-\mathbf{q}) + (J_{\mathbf{q}}-J_\perp)^2\chi^-(\mathbf{q})\mathcal{G}_{s,w}^{(B,A)}(\mathbf{k}-\mathbf{q})], \quad (3)$$

where, the + (−) sign is for the normal (abnormal) self-energy $\Sigma_{s(w)}$ and the symbol $\mathbf{q}$ represents an abbreviation of $\mathbf{q},i\omega_m$. The renormalized Green's function is $G^{(A,B)}(\mathbf{k},i\omega)=\{[G_s^{(A,B)}(\mathbf{k},i\omega)]^{-1}+(\Delta_{\mathbf{k}}+\Sigma_w^{(A,B)})^2G_s^{(A,B)}(\mathbf{k},-i\omega)\}^{-1}$ with $G_s^{(A,B)}=[i\omega-\epsilon^{(A,B)}-\Sigma_s^{(A,B)}]^{-1}$, and the spectral function is obtained via $A(k,\omega)=-(1/\pi)\mathrm{Im}[G(k,\omega+i\delta)]$. To determine the QP weight z, we first write the Green's function as $G(\mathbf{k},i\omega)=M/(i\omega+\Sigma_\alpha)+N/(i\omega-\Sigma_\beta)$ and get z via $z=M/[1+\partial\Sigma_\alpha/\partial\omega(\omega_0)]$, with ω_0 the pole of G. The parameters we choose are $t=2J$, $t'=-0.7t$, $J=120$ meV, and $J_\perp=0.1J$.[15] Except in Fig. 4 the doping density is set at $\delta=0.2$.

Figures 1(a) and 1(b) display the calculated QP dispersion for the BB band obtained from the momentum distribution curve[16] (MDC) in the antinodal and nodal regions, respectively. One can see from Fig. 1(a) that the antinodal kink appears in some range of parameters t_p and α, such as $t_p=2.0J$ and $\alpha=0.43$. The RPA correction factor $\alpha=0.34$, 0.43, and 0.55 corresponds to the critical doping density of the AF instability $\delta_c=0.02$, 0.05, and 0.09, while $\delta_c=0.02-0.05$ is within the experimental range.[15] Meanwhile, the ARPES experiment indicated that $t_{\perp,expt}$ (corresponding to δt_p, $\delta\sim0.2$) is 44±5 meV (Ref. 17)—i.e., $t_p=(1.6-2.0)J$ here. Therefore, in a reasonable parameter range, the interaction between fermions and SF reproduces well the observed antinodal kink. In contrast, Fig. 1(b) shows that no kink is present in the nodal region. This can be understood from the conservation of the momentum in the scattering process; namely, the nodal-to-nodal scattering involves a smaller transferred momentum than $\mathbf{Q}=(\pi,\pi)$ where the AF spin fluctuation peaks. Thus, we will focus mainly on the antinodal region in the following discussion. In Fig. 1(c) we replot the MDC dispersion together with the EDC derived dispersion.[16] Near and below the region where the kink appears in the MDC dispersion, the EDC dispersion breaks into a two-part structure, a peak and a hump. Therefore, the appearance of the antinodal kink has an intimate relation to the PDH structure in the EDC plot, being in agreement with experiments.[18]

In fact, the kink may also be expected if fermions are predominantly coupled to other collective modes. A hotly discussed mode responsible for the antinodal kink is the out-of-plane out-of-phase O bucking B_{1g} phonon.[9,10] To take into account this kind of mode, we may have the total Hamil-

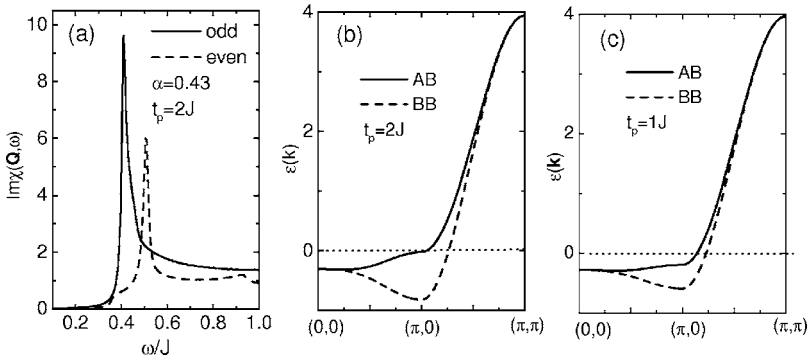

FIG. 2. (a) Im $\chi(\mathbf{q},\omega)$ vs ω at (π,π). (b) and (c) show the bare dispersion of the normal-state quasiparticle for $t_p=2J$ and $1.0J$, respectively.

tonian by including the following interaction in the slave-boson mean field Hamiltonian H_m:

$$H_{ep}=\frac{1}{\sqrt{N}}\sum_{\mathbf{kq}\alpha\sigma} g(\mathbf{k},\mathbf{q}) f^{(\alpha)\dagger}_{\mathbf{k},\sigma} f^{(\alpha)}_{\mathbf{k}+\mathbf{q},\sigma}(d^{\dagger}_{\mathbf{q}}+d_{-\mathbf{q}}), \tag{4}$$

where $d^{\dagger}$ and d are the creation and annihilation operators for phonons, $g(\mathbf{k},\mathbf{q})=g_0[\Phi_x(\mathbf{k})\Phi_x(\mathbf{k}-\mathbf{q})\cos(q_y/2)-\Phi_y(\mathbf{k})\Phi_y(\mathbf{k}-\mathbf{q})\cos(q_x/2)]/\sqrt{\cos^2 q_x/2+\cos^2 q_y/2}$, and the detailed form of Φ_x,Φ_y can be found in Refs. 9 and 10. We note that the vertex $g(\mathbf{k},\mathbf{q}=0)\sim\cos(k_x)-\cos(k_y)$ and vanishes for all $\mathbf{k}$ at $\mathbf{q}=(\pi,\pi)$.[9,10] Thus, the fermions near $(\pi,0)$ are strongly scattered by this interaction. The corresponding fermionic self-energy for both bands is given by

$$\Sigma_{s,w}(\mathbf{k})=\pm\frac{1}{\beta N}\sum_{\mathbf{q}}|g(\mathbf{k}-\mathbf{q},\mathbf{q})|^2 D_0(\mathbf{q}) \times[\mathcal{G}^{(A)}_{s,w}(\mathbf{k}-\mathbf{q})+\mathcal{G}^{(B)}_{s,w}(\mathbf{k}-\mathbf{q})], \tag{5}$$

where the Green's function of the phonon is $D_0(\mathbf{q})=2\omega_q/[(i\omega)^2-(\omega_q)^2]$ and a dispersionless optical phonon (B_{1g}) will be taken as $\hbar\omega_q=36$ meV.[9,10] We determine the coupling constant g_0 as the values which give rise to a well-established antinodal kink and find that $g_0\approx 0.2J-0.4J$ if $t_p=1.7J$. The result is shown in Fig. 1(d), it is quite similar to that for the SF in Fig. 1(a). So a mere reproduction of the QP kink is not sufficient to single out the main cause of the renormalization, and we must resort to other features.

A meaningful difference between the effects of these two interactions on the dispersion can be seen clearly from a comparison of Figs. 1(a) and 1(d); namely, the interlayer coupling t_p has an opposite effect on the antinodal kink. It enhances the kink feature for the fermion-SF interaction; as shown in Fig. 1(a), when t_p decreases to $1.7J$, no antinodal kink is observed even for the strongest AF coupling $\alpha=0.55$ which is in fact beyond the experimentally acceptable value. In contrast, the kink feature is weakened by the interlayer coupling for the fermion-phonon interaction; as seen in Fig. 1(d), the kink disappears when t_p increases to $2J$ from $1.7J$ with $g_0=0.2J$. Recent ARPES experiments revealed that a more pronounced kink is present in the multilayered BiSrCaCuO, in contrast to the case in the single-layered one,[4] which can be considered as an indication to favor the fermion-SF interaction in the bilayer system. Because the spin susceptibility in the bilayer system involves scatterings between layers, the self-energy [Eq. (3)] has a feature that the fermions in the BB (AB) band is scattered into AB (BB) band via the SF in the odd channel χ^{-}. The so-called spin resonance (a sharp peak in Im χ) appears around $\mathbf{Q}$ both in the odd χ^{-} and even χ^{+} channels [see Fig. 2(a)]. However, it is more prominent in the odd channel, which is in agreement with very recent experiments,[19] mainly due to the larger vertex $\alpha J_{\mathbf{Q}}-J_{\perp}$ $(J_{\mathbf{Q}}=-2J)$ [Eq. (2)], compared to $\alpha J_{\mathbf{Q}}+J_{\perp}$ in the even channel. On the other hand, the AB band (and its associated flatband near $\mathbf{Q}$) is much close to the Fermi surface compared to the BB band, as shown in Fig. 2(b). As a result, the fermionic self-energy for BB band is large, and consequently the renormalization is strong. We have indeed observed that the AB band is much less affected, so no kink is present in this band (not shown here). As increasing t_p, the splitting between the AB and BB band pushes the flat portion

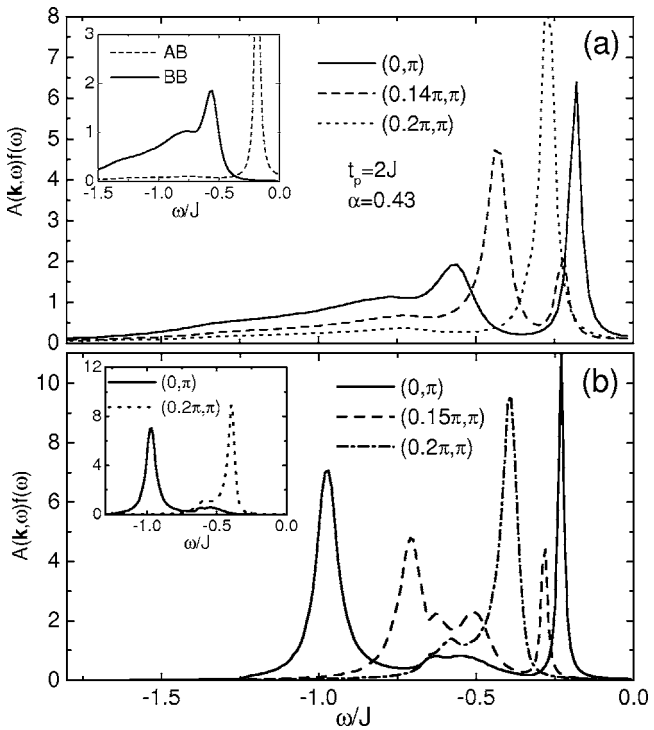

FIG. 3. The line shape of fermions at different k points. (a) is obtained when fermions are coupled to spin fluctuations. (b) shows the result arising from the coupling to the B_{1g} phonons. The inset in (a) shows the line shape for the bonding and antibonding bands at $(0,\pi)$, separately. The inset in (b) is the line shape for the bonding band at $\mathbf{k}=(0,\pi)$ and $(0.2\pi,\pi)$.

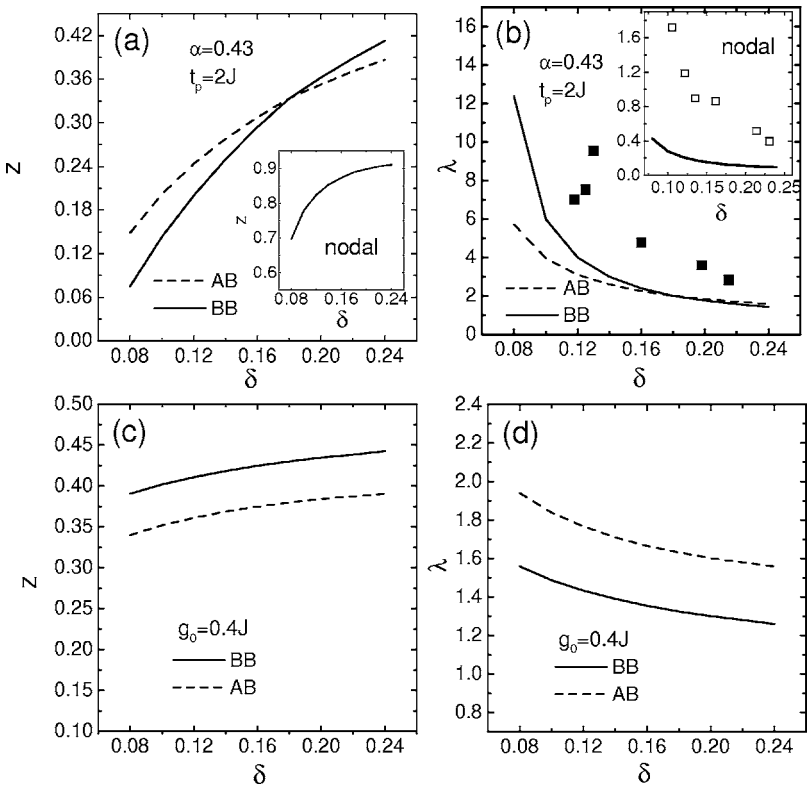

FIG. 4. The quasiparticle weight z of fermions and its coupling constant λ at the antinodes arising from the coupling to spin fluctuations (a),(b) and to phonons (c),(d). The insets show those at the nodes. The scattered points are experimental data from Refs. 3 and 6, respectively.

of the AB band to be more close to the Fermi level [Figs. 2(b) and 2(c)], so enhances the scattering. However, for the coupling to phonons, the AB and BB bands contribute to the self-energy in the same way [Eq. (5)]. In this case, though the increase of t_p increases the contribution from the AB band, the decrease from the BB band overcompensates that increase, and thus the self-energy decreases with t_p on the whole.

In Fig. 3, we show the line shape for different k points from $(0,\pi)$ to $(0.2\pi,\pi)$. For the fermion-SF interaction, both the BB and AB spectra near $(0,\pi)$ consist of a low-energy peak, followed by a hump, and then a dip in between, though the intensity of the AB hump is much weaker than its peak intensity [inset of Fig. 3(a)]; both develop their own PDH structure near $(0,\pi)$. When moving from $(0,\pi)$ to $(0.2\pi,\pi)$, one will see that the intensity of the BB peak increases, while the AB peak decreases rapidly. Eventually, only the BB peak can be seen near $(0.2\pi,\pi)$. These features are in good agreement with ARPES experiments.[17] However, the line shape caused by the phonon-coupling displays a striking contrast to those shown in Fig. 3(a) and in experiments;[17] namely, the peak is far below the dip and the dip is below the hump [Fig. 3(b)]. This is because the renormalization to the QP peak in the BB band due to the phonons is rather weak, so the peak changes a little comparing to the bare one. It also differs from the case of the single-layered system,[20] because the interlayer coupling t_p here pushes the BB band to be much deeper inside the Fermi sea. When moving from $(0,\pi)$ to $(0.2\pi,\pi)$, the QP moves to be near the Fermi level and the hump arising from the phonon coupling does not change, so an ordinary PDH structure is recovered at $(0.2\pi,\pi)$ [inset of Fig. 3(b)].

Figure 4 presents the QP weight z of fermions and the coupling constant λ. Notice that the weight of the physical electron is δz due to the condensation of holons in the slave-boson approach.[13] For the fermion-SF interaction, the weight at $(0,\pi)$ decreases rapidly with underdoping, from nearly 0.42 and 0.39 at doping $\delta=0.24$ (the bare value is 0.5) to be below 0.075 and 0.15 at $\delta=0.08$ for the BB and AB bands, respectively. On the other hand, the weight along the nodal direction decreases very slowly, and it is still 0.7 even at $\delta=0.08$. This exhibits a highly anisotropic interaction between fermions and SF and is well consistent with what is inferred from ARPES (Ref. 5) and a recent argument based on the analysis of experimental data.[21] Moreover, the coupling constant obtained using $z=1/(1+\lambda)$ shows a reasonable fit to experimental data[3] [Fig. 4(b)], while that at the nodal direction is much smaller than the experimental data[6] [inset of Fig. 4(b)]. This consistency is significant, because we use the well-established parameters in the t-t'-J model with only one adjustable parameter α being fixed by fitting to experiments. In contrast, the weight decreases much slowly for the fermion-phonon interaction as shown in Fig. 4(c), and the coupling constant λ is nearly 3–5 times smaller than experimental values.

Finally, we wish to make two additional remarks. First, because the spin resonance contributes little to the node-to-node scattering, a kink structure in the nodal direction should be caused by the other mode coupling, such as an in-plane Cu-O breathing phonon.[1] The different momentum, temperature, and doping dependence between the nodal and antinodal kink [feature (iv)] supports this point of view. Second, since the interlayer coupling plays opposite roles in the antinodal kink, respectively, for the fermion-SF and fermion-phonon interactions, it is expected that, even though a rather

weak fermion-phonon coupling may be present and lead to a weak antinodal kinklike behavior in the single-layered cuprates, as possibly seen in the experiment for Bi2201,[4] the coupling is too weak to affect significantly the line shape which is mainly determined by the SF as shown in Ref. 14.

We are grateful to F.C. Zhang for many useful discussions. The work was supported by the NNSFC (Grant Nos. 10474032, 10429401, and 10334090), the RGC of Hong Kong (Grant No. HKU 7050/03P), the URC fund of HKU, the Ministry of Science and Technology of China (973 project Grant No. 2006CB601002, and partly by RFDP (Grant No. 20030284008).

[1] A. Lanzara, P. V. Bogdanov, X. J. Zhou, S. A. Kellar, D. L. Feng, E. D. Lu, T. Yoshida, H. Eisaki, A. Fujimori, K. Kishio, J.-I. Shimoyama, T. Noda, S. Uchida, Z. Hussain, and Z. X. Shen, Nature (London) **412**, 510 (2001).

[2] S. V. Borisenko, A. A. Kordyuk, T. K. Kim, A. Koitzsch, M. Knupfer, M. S. Golden, J. Fink, M. Eschrig, H. Berger, and R. Follath, Phys. Rev. Lett. **90**, 207001 (2003); A. D. Gromko, A. V. Fedorov, Y. D. Chuang, J. D. Koralek, Y. Aiura, Y. Yamaguchi, K. Oka, Y. Ando, and D. S. Dessau, Phys. Rev. B **68**, 174520 (2003).

[3] T. K. Kim, A. A. Kordyuk, S. V. Borisenko, A. Koitzsch, M. Knupfer, H. Berger, and J. Fink, Phys. Rev. Lett. **91**, 167002 (2003).

[4] T. Sato, H. Matsui, T. Takahashi, H. Ding, H. B. Yang, S. C. Wang, T. Fujii, T. Watanabe, A. Matsuda, T. Terashima, and K. Kadowaki, Phys. Rev. Lett. **91**, 157003 (2003).

[5] A. Damascelli, Z. Hussain, and Z. X. Shen, Rev. Mod. Phys. **75**, 473 (2003).

[6] P. D. Johnson, T. Valla, A. V. Fedorov, Z. Yusof, B. O. Wells, Q. Li, A. R. Moodenbaugh, G. D. Gu, N. Koshizuka, C. Kendziora, S. Jian, and D. G. Hinks, Phys. Rev. Lett. **87**, 177007 (2001).

[7] H. F. Fong, B. Keimer, P. W. Anderson, D. Reznik, F. Dogan, and I. A. Aksay, Phys. Rev. Lett. **75**, 316 (1995).

[8] P. Bourges, Y. Sidis, H. F. Fong, L. P. Regnault, J. Bossy, A. Ivanov, and B. Keimer, Science **288**, 1234 (2000).

[9] T. Cuk, F. Baumberger, D. H. Lu, N. Ingle, X. J. Zhou, H. Eisaki, N. Kaneko, Z. Hussain, T. P. Devereaux, N. Nagaosa, and Z. X. Shen, Phys. Rev. Lett. **93**, 117003 (2004).

[10] T. P. Devereaux, T. Cuk, Z. X. Shen, and N. Nagaosa, Phys. Rev. Lett. **93**, 117004 (2004).

[11] M. Eschrig and M. R. Norman, Phys. Rev. Lett. **89**, 277005 (2002).

[12] O. K. Anderson, A. I. Liechtenstein, O. Jepsen, and F. Paulsen, J. Phys. Chem. Solids **56**, 1573 (1995); T. Xiang and J. M. Wheatley, Phys. Rev. Lett. **77**, 4632 (1996).

[13] P. A. Lee, Physica C **317-318**, 194 (1999); J. Brinckmann and P. A. Lee, Phys. Rev. Lett. **82**, 2915 (1999).

[14] J. X. Li, C. Y. Mou, and T. K. Lee, Phys. Rev. B **62**, 640 (2000).

[15] A. P. Kampf, Phys. Rep. **249**, 219 (1994).

[16] Besides MDC, another intensity plot in ARPES is the energy distribution curve (EDC). Due to the abnormal line shape of EDC (Ref. 5), MDC is more often used to analyze the dispersion.

[17] D. L. Feng, N. P. Armitage, D. H. Lu, A. Damascelli, J. P. Hu, P. Bogdanov, A. Lanzara, F. Ronning, K. M. Shen, H. Eisaki, C. Kim, Z. X. Shen, J.-i. Shimoyama, and K. Kishio, Phys. Rev. Lett. **86**, 5550 (2001).

[18] M. R. Norman, M. Eschrig, A. Kaminski, and J. C. Campuzano, Phys. Rev. B **64**, 184508 (2001).

[19] S. Pailhes, Y. Sidis, P. Bourges, C. Ulrich, V. Hinkov, L. P. Regnault, A. Ivanov, B. Liang, C. T. Lin, C. Bernhard, and B. Keimer, Phys. Rev. Lett. **91**, 237002 (2003).

[20] A. W. Sandvik, D. J. Scalapino, and N. E. Bickers, Phys. Rev. B **69**, 094523 (2004); R. Zeyher and A. Greco, *ibid.* **64**, 140510(R) (2001).

[21] D. E. Sheehy, T. P. Davis, and M. Franz, Phys. Rev. B **70**, 054510 (2004).